Phase equilibrium of the CO2/glycerol system: Experimental data by in situ FT-IR spectroscopy and thermodynamic modeling

Yaocihuatl Medina-Gonzalez, Thierry Tassaing, Séverine Camy, Jean-Stéphane Condoret

Phase equilibrium of the CO_2/glycerol system: Experimental data by *in situ* FT-IR spectroscopy and thermodynamic modeling

Y. Medina-Gonzalez[a,b,c,1,2], T. Tassaing[c,*], S. Camy[a,b,1], J.-S. Condoret[a,b,**]

[a] *Université de Toulouse, INPT, UPS, Laboratoire de Génie Chimique UMR CNRS 5503, 4, Allée Emile Monso, F-31030 Toulouse, France*
[b] *CNRS, Laboratoire de Génie Chimique, F-31432 Toulouse, France*
[c] *Institut de Sciences Moléculaires, UMR 5255 CNRS, Université Bordeaux, 351, cours de la Libération, 33405 Talence Cedex, France*

A B S T R A C T

Phase equilibrium experimental data for the CO_2/glycerol system are reported in this paper. The measurements were performed using an *in situ* FT-IR method for temperatures ranging from 40 °C to 200 °C and pressures up to 35.0 MPa, allowing determination of the mutual solubility of both compounds. Concerning the CO_2 rich phase, it was observed that the glycerol solubility in CO_2 was extremely low (in the range of 10^{-5} in mole fraction) in the pressure and temperature domains investigated here. Conversely, the glycerol rich phase dissolved CO_2 at mole fractions up to 0.13. Negligible swelling of the glycerol rich phase has been observed. Modeling of the phase equilibrium has been performed using the Peng–Robinson equation of state (PR EoS) with classical van der Waals one fluid and EoS/G^E based mixing rules (PSRK and MHV2). Satisfactory agreement was observed between modeling results and experimental measurements when PSRK mixing rules are used in combination with UNIQUAC model, although UNIFAC predictive approach gives unsatisfactory representation of experimental behavior.

Keywords:
Glycerol
Supercritical CO_2
Biphasic system
Phase equilibrium
Infrared spectra
Thermodynamic modeling

1. Introduction

Recently, interest in biphasic systems, which couple supercritical CO_2 and a conventional liquid solvent have been highlighted [1,2], as they can provide innovative reaction media. The interest of these biphasic systems is maximum when the partner solvent is a biosourced solvent because such systems become then environmentally friendly. Such biphasic systems are useful to overcome the limited solvating power of pure $scCO_2$, especially in respect to homogeneous catalysis where in this case catalysts can be more easily solubilized in the liquid solvent. They can also alleviate the drawback of the conventional use of biosourced solvents whose low volatility usually handicaps easy recovery of the reaction products. Indeed, supercritical CO_2 can be used to recover the reaction products by extraction from the liquid phase. In addition, these biphasic systems can be considered as intensified systems because, in this case, reaction and separation are operated in one single step.

Among the biosourced solvents, glycerol is of prime interest as it is a byproduct in biodiesel fabrication and it is therefore very easily available. Provided its potential own chemical reactivity is not problematic, glycerol can be proposed as an alternative reaction medium for water, when water is not suitable due to its hydrolytic power or in the case of dehydration reactions for instance. Glycerol has been shown to be an interesting alternative for different organic synthesis [3,4] as for instance selective reduction of aldehydes, ketones and β-ketoesters with $NaBH_4$ [5]. Several other examples have been gathered in a review by Diaz-Alvarez et al. [6]. Studies by Jérôme and Gu [7–9], have shown that, in some reactions, such as the Aza-Michael reaction of p-anisidine and the Michael reaction of indole, glycerol used as solvent is capable to achieve yields up to 80% under catalyst-free conditions, these yields being higher than those obtained with usual solvents. The same research group has developed a series of catalysts combined with sugar-based-surfactants of organic substrates which favors mass transfer of organic substrates and limits the undesired reactivity of glycerol [10]. However, drawbacks in the utilization of non-volatile solvents, such as glycerol, are still the uneasy recovery of products and recycling of catalysts. In this context, biphasic systems using supercritical CO_2 ($scCO_2$) as a partner phase make it possible the solubilization of the catalyst in the glycerol phase while products are extracted by $scCO_2$ [9,11,12].

In this context, one prerequisite for effective design and control of such biphasic systems is the knowledge of the phase equilibrium

* Corresponding author. Tel.: +33 05 40 00 28 92; fax: +33 05 40 00 84 02.
** Corresponding author at: Université de Toulouse, INPT, UPS, Laboratoire de Génie Chimique UMR CNRS 5503, 4, Allée Emile Monso, F-31030 Toulouse, France. Tel.: +33 05 34 32 36 97; fax: +33 05 34 32 37 07.
E-mail addresses: t.tassaing@ism.u-bordeaux1.fr (T. Tassaing), jeanstephane.condoret@ensiacet.fr (J.-S. Condoret).
[1] Tel.: +33 05 34 32 37 13; fax: +33 05 34 32 37 07.
[2] Tel.: +33 05 34 32 36 70; fax: +33 05 34 32 36 97.

http://dx.doi.org/10.1016/j.supflu.2012.11.012

of the mixture. Also, understanding the effects of dissolved CO_2 on the physicochemical properties of the glycerol-rich phase is important for reaction design [13,14]. Indeed, CO_2 modifies the polarity of the solvent and, for instance, from this effect, initially miscible compounds are likely to become immiscible when the solvent is pressurized with CO_2, even at moderate pressures (5.0 MPa) [15]. So, CO_2 can then act as a switch to control the polarity and solvating properties of the partner solvent, allowing recovery of catalysts, products, byproducts, and so on. Despite this recent growing interest for $scCO_2$/glycerol system, phase equilibrium experimental data are scarce and not yet fully validated. Only two studies upon experimental determinations of solubility of glycerol in pressurized CO_2 have been published [16,17] and their results are not in coherence. To perform accurate measurements of concentrations of the phases in equilibrium, the technique of *in situ* FTIR spectroscopy can be proposed. This method has been previously successfully applied in phase equilibrium studies for the determination of the CO_2 sorption and swelling in liquids [18,19] and in polymers [20,21]. In particular, we would like to stress that molar absorption coefficients of CH–stretching vibrational modes and combination bands are expected to exhibit little sensitivity upon temperature and pressure conditions [20,22,23]. For example, Buback et al. [24] have shown that the molar absorption coefficient of combination bands of CO_2 were almost independent of the CO_2 density. Therefore, IR spectroscopy allows determining the concentration of a given specie in a mixture with a statistical error lower than 10%.

Also, modeling of $scCO_2$–glycerol phase equilibrium has been already proposed [25] but the lack of experimental results did not allow validation of the model. Such calculations are useful but accurate prediction of CO_2–glycerol phase equilibrium has not been yet fully developed and compared with experimental results.

In this context, the purpose of the present work is to experimentally determine the phase behavior of the CO_2/glycerol system using *in situ* FTIR spectroscopy and to propose an adequate thermodynamic modeling of the phase equilibrium data.

2. Experimental

2.1. Materials

Dry glycerol with purity of ≥99.5% was purchased from Sigma–Aldrich; water content was determined by titration with a Mettler-Toledo DL38 Karl–Fischer titrator and found to be 0.04%. CO_2 N45 was obtained from Air Liquide. All chemicals were used without further purification. A BioRad FTS-60A interferometer equipped with a globar as infrared source, a KBr/Ge beamsplitter and a DTGS (deuterated triglycine sulfate) detector has been employed to record single beam spectra in the range of 400–6000 cm^{-1}. Single beam spectra recorded with 2 cm^{-1} resolution were obtained from the Fourier transformation of 30 accumulated interferograms.

2.2. Apparatus and procedure

The high-pressure cell and the infrared setup used for phase behavior determination experiments have been described thoroughly elsewhere [18]. Solubility of glycerol in CO_2 has been determined using a cell with an optical path length of 25.3 mm and equipped with germanium windows, employing the following procedure: bottom of the cell was filled with dry glycerol and a magnetic bar was placed inside. The cell was tightly closed then placed inside the interferometer and thermostated at the desired temperature using cartridge heaters. CO_2 was pumped inside the cell to the desired pressure and the system was agitated using a magnetic stirrer. After an equilibration period of at least 3 h, FT-IR spectra of the CO_2 rich phase were obtained. During the stabilization of the operating conditions (weak decrease of the pressure between 1 and 10 bar that was compensated with the manual pump), consecutive spectra were recorded every 30 min. Equilibrium has been considered as reached when at least three consecutive spectra spaced by 30 min did not show any significant absorbance difference. Indeed, as a consequence of the high viscosity of glycerol, it has been observed that equilibration period was temperature dependent and decreased sharply with temperature: at low temperatures (40 °C) equilibration needed about 120 h. Two series of measurements have been performed for a number of points in specified conditions of temperature and pressure to check for the reproducibility of the measurements.

Table 1
Molar extinction coefficients of glycerol and CO_2 for different absorption bands.

	Glycerol		CO_2
Group frequency	ν_{C-H}	ν_{C-H}	$2\nu_2 + \nu_3$
Wave number (cm^{-1})	2933	2883	3696
ε ($L\,mol^{-1}\,cm^{-1}$)	49.78	47.61	10.978

CO_2 solubility in glycerol was determined using the same system by filling the cell with dry glycerol. The optical path length was fixed to 0.12 mm and sapphire windows were used for this determination. FT-IR spectra of the glycerol-rich phase have then been acquired. Solubility experiments were performed at temperatures ranging from 40 to 200 °C and pressures up to 35 MPa.

2.3. Data processing for the determination of mutual solubility and phase equilibrium

Beer–Lambert law ($A = \varepsilon \cdot L \cdot c$, where A is the sample absorbance, ε the molar extinction coefficient ($L\,mol^{-1}\,cm^{-1}$), L the optical path length (cm) and c the sample concentration ($mol\,L^{-1}$)) was used to calculate the concentrations of glycerol and CO_2 in each phase. In order to determine the concentration of glycerol in the CO_2-rich phase, the absorbance of the two peaks centered at about 2933 and 2883 cm^{-1} associated to the νCH stretching mode of glycerol was used.

As baseline correction can induce large errors when peak integrated area is used for quantification, peak height was used for these determinations in order to minimize this error. In order to determine the concentration of glycerol ($C_{glycerol}$) in the CO_2-rich phase, molar extinction coefficients (ε) for two selected bands of glycerol were determined from spectra of aqueous solutions of glycerol at known concentrations (see Table 1). We emphasize that the signal of the FTIR spectrum of glycerol in the C–H stretching region was the same in water and in CO_2 which shows, as it is expected, that the C–H stretching vibrational modes of glycerol are not sensitive to the nature of the solvent. Thus, the concentrations were calculated from the average of the concentration values estimated with the two considered CH peaks of glycerol (see Table 1).

In order to determine the CO_2 concentration (C_{CO_2}) in the glycerol-rich phase, the peak height of the $2\nu_2 + \nu_3$ band of CO_2 centered at 3696 cm^{-1} was used. Molar extinction coefficient of this band was determined by recording the infrared spectra of neat CO_2 at different temperatures and pressures, the density (concentration) was then obtained from literature [26]. Table 1 shows the obtained ε value.

Mole fraction of glycerol in the CO_2-rich phase has been calculated as:

$$x_{glycerol} = \frac{C_{glycerol}}{C_{glycerol} + C_{CO_2}} \quad (1)$$

where $C_{glycerol}$ is the concentration of glycerol as determined by our FTIR measurements and C_{CO_2} is calculated from the NIST data [26].

Table 2
Density of pure glycerol at atmospheric pressure as function of temperature.

T (°C)	Density (kg/m^3)[a]	Density (kg/m^3)	Relative difference[c]
40	1272.3	1248[b]	0.019
60	1281.3	1235[b]	0.036
80	1259.2	1223[b]	0.029
100	1209.3	1209.27[b]	2.5E−5
120	1189.7	1194.46[c]	0.004
140	1163.6	1179.51[c]	0.013
160	1131.0	1164.4[c]	0.029
180	1116.0	1148.64[c]	0.028
200	1083.1	1131.78[c]	0.043

[a] Data from this study (precision ±5%).
[b] Data from Ref. [27].
[c] Data from Ref. [48]. Calculated as $\frac{|obtained\ \ value - literature\ \ value|}{literature\ \ value}$.

Indeed, as the solubility of glycerol in the CO_2 rich phase is very low (see below), it has been considered that the concentration of CO_2 in the CO_2 rich phase was not affected by the presence of glycerol and equal to that of neat CO_2 under the same temperature–pressure conditions.

Mole fraction of CO_2 in the glycerol-rich phase was obtained from:

$$x_{CO_2} = \frac{C_{CO_2}}{C_{CO_2} + C_{glycerol}} \tag{2}$$

where C_{CO_2} is the concentration of absorbed CO_2 in the glycerol rich-phase determined by our FTIR measurements and $C_{glycerol}$ is the concentration of neat glycerol obtained from FTIR measurement performed on neat glycerol as a function of temperature (see below). Indeed, as it will be evidenced below in Section 3.2, significant swelling of the glycerol rich phase by $scCO_2$ was not detected in the range of temperature and pressure investigated here. Therefore, it was assumed that the concentration of glycerol in the glycerol rich phase was equal to that of neat glycerol under the same temperature conditions. Glycerol density at atmospheric pressure has been calculated as a function of temperature from pure glycerol spectra, by using the peak centered at about 5700 cm^{-1}, which was assigned to $2\nu_{C-H}$. Thus, using the Beer–Lambert law, the concentration (density) of neat glycerol was calculated using the peak height of the band observed at 5700 cm^{-1} associated with the $2\nu_{C-H}$ overtone. To determine the molar extinction coefficient ε for this mode, the spectrum measured at T = 100 °C was used as a reference and the corresponding concentration data reported in the literature at the same temperature [27]. The concentration (density) values of neat glycerol calculated using this method are shown in Table 2 and good agreement with values reported in the literature [27] can be observed, relative difference between both values is presented as well. The present values of density have then been used to calculate the concentration of the glycerol-rich phase.

Finally, taking into account all the source of errors associated with our methodology (baseline correction, constant molar extinction coefficient, spectrometer stability), a maximum relative error of about ±5% in the concentration values has been estimated. We emphasize that the reliability of such methodology has already been demonstrated in previous investigations on the mutual solubility of epoxide with CO_2 [19] and water with CO_2 [23] where a satisfactory agreement with literature data was shown.

2.4. Phase equilibrium modeling

Thermodynamic modeling was performed using the well-known Peng–Robinson equation of state (PR EoS) [28], *i.e.*, with a different expression of the m_i term for compounds with acentric factor greater that the one of n-decane (0.491) [29], as it is the case for glycerol. In a first approach, Peng–Robinson EoS has been used with the classical van der Waals one-fluid mixing rule (vdW1f) for a and b parameters. Classical combining rules, *i.e.*, geometric mean rule with k_{ij} binary interaction coefficient for a_{ij} parameter, and arithmetic mean rule, without any interaction coefficient, for b_{ij} parameter have been used. Finally, a and b parameters of the mixture are obtained from the following equations:

Table 3
Characteristic parameters of pure compounds used in PR EoS.

Compound	T_c (K)	P_c (MPa)	ω	M (kg kmol^{-1})
CO_2 [49]	304.21	7.38	0.2236	44.01
Glycerol [50]	850	7.5	0.516	92.09

$$a(T) = \sum_{i=1}^{n}\sum_{j=1}^{n} z_i z_j \sqrt{a_i a_j}(1 - k_{ij}) \tag{3}$$

$$b = \sum_{i=1}^{n} z_i b_i \tag{4}$$

with

$$a_i = 0.457235529 \cdot \frac{R^2 T_{c,i}^2}{P_{c,i}} \cdot \alpha_i(T) \tag{5}$$

$$b_i = 0.0777960739 \cdot \frac{R T_{c,i}}{P_{c,i}} \tag{6}$$

The computation procedure for the parameter $\alpha_i(T)$ depends on the temperature and acentric factor values of the compound. For compounds above their critical temperature, $\alpha_i(T)$ is calculated as recommended by Boston and Mathias [30]:

$$\alpha_i(T) = [\exp[c_i(1 - T_{r,i}^{di})]]^2 \tag{7}$$

with

$$d_i = 1 + \frac{m_i}{2} \tag{8}$$

$$c_i = 1 - \frac{1}{d_i} \tag{9}$$

$$\text{if}\ \ \omega_i \le 0.491\ \ \text{then}\ \ m_i = 0.37464 + 1.54226\omega_i - 0.26992\omega_i^2 \tag{10}$$

$$\text{if}\ \ \omega_i > 0.491\ \ \text{then}\ \ m_i = 0.379642 + 1.48503\omega_i - 0.164423\omega_i^2 + 0.016666\omega_i^3 \tag{11}$$

Else, if $T < T_{c,i}$, the conventional expression of $\alpha_i(T)$ for Peng–Robinson is used:

$$\alpha_i(T) = [1 + (0.37464 + 1.54226\omega_i - 0.26992\omega_i^2)(1 - \sqrt{T_{r,i}})]^2 \quad \text{if}\ \ \omega_i \le 0.491 \tag{12}$$

$$\alpha_i(T) = [1 + (0.379642 + 1.48503\omega_i - 0.164423\omega_i^2 + 0.016666\omega_i^3)(1 - \sqrt{T_{r,i}})]^2 \quad \text{if}\ \ \omega_i > 0.491 \tag{13}$$

Pure component properties of CO_2 and glycerol necessary for these calculations are presented in Table 3.

Carbon dioxide and glycerol exhibit very different polarity and the so-called EoS/G^E approach is then expected to be more appropriate to model high-pressure fluid phase equilibria of this system. Indeed, this kind of mixing rules enlarges the field of application of

Table 4
Summary of the models used in this work to represent CO_2–glycerol phase equilibrium.

Name of the global model	Equation of state	Mixing rule	Activity coefficient model	Binary interaction coefficients
PR	PR	Conventional	–	$k_{ij} = f(T)$
PSRK-UNIFAC	PR	PSRK	UNIFAC PSRK	–
PSRK-UNIQUAC	PR	PSRK	UNIQUAC	$A_{ij} = f(T)/A_{ji} = f(T)$
MHV2-UNIFAC	PR	MHV-2	UNIFAC Lyngby	–
MHV2-UNIQUAC	PR	MHV-2	UNIQUAC	$A_{ij} = f(T)/A_{ji} = f(T)$

cubic equation of state to polar compounds at high pressure. This is done *via* the incorporation of the excess Gibbs energy (G^E) in the calculation of the energy parameter, a, of the EoS. The excess Gibbs energy is calculated using an activity coefficient model. Huron and Vidal [31] were the first to propose this approach, and several models based on this concept have then been developed, such as Wong-Sandler, MHV1, MHV2, PSRK. . .and were successfully applied to describe high pressure fluid phase equilibria of mixtures containing polar compounds ([32,33] as examples). A complete review of EoS/G^E mixing rules and their range of application can be found in the recent book of Kontogeorgis and Folas [34].

For the purpose of this study PSRK [35] and MHV2 [36,37] mixing rules have been chosen, in addition to classical vdWf1 mixing rules. Their ability to model the CO_2–glycerol thermodynamic behavior has been compared. For both PSRK and MHV2 mixing rules, Peng–Robinson has been used as the equation of state and Eqs. (4)–(13) have been used to evaluate pure component parameters and to calculate mixture parameter b of the PR EoS.

For PSRK and MHV2, mixture parameters are obtained from:

$$q_1\left(\alpha - \sum_i z_i\alpha_i\right) + q_2\left(\alpha^2 - \sum_i z_i\alpha_i^2\right) = \frac{g_0^E}{RT} + \sum_i z_i \ln\left(\frac{b}{b_i}\right) \tag{14}$$

$$\alpha = \frac{a}{bRT} \tag{15}$$

$$\alpha_i = \frac{a_i}{b_iRT} \tag{16}$$

with a_i, b_i and b obtained from (5), (6) and (4) respectively. In the case of Peng–Robinson equation of state, $q_1 = 0.64663$ and $q_2 = 0$ for PSRK model (explicit calculation of α) and $q_1 = -0.4347$ and $q_2 = -0.003654$ for MHV2 model (implicit calculation of α). Then an activity coefficient model has to be chosen to determine the value of the excess Gibbs energy at zero pressure (reference pressure) g_0^E. At their initial development, authors of PSRK, so as MHV mixing rules, coupled the SRK or PR equation of state with the UNIFAC predictive activity coefficient model, leading to a predictive way to use cubic equations of state. In the present study, PSRK mixing rule has been used with the PSRK version of UNIFAC model proposed by Fredenslund et al. [38] and modified in such a way that binary interaction coefficients between functional groups depend on temperature [35,39] and with UNIQUAC activity coefficient model [40,41]. In a same way, MHV2 mixing rule is used with the Lingby version of UNIFAC [42]. When UNIQUAC model is used in the mixing rule, two binary interaction coefficients (A_{ij} and A_{ji}) have to be fitted on experimental data. In the present study, because of the large range of investigated temperatures, binary interaction coefficients have been shown to be linearly temperature dependent. Fluid phase equilibria calculations have been performed using Excel (Microsoft) coupled with Simulis® Thermodynamics software (ProSim S.A, France). Simulis® Thermodynamics contains the different models summarized in Table 4. Relative absolute average deviation (expressed in percentage, *%AAD*) was calculated to evaluate ability of the model to represent experimental data for CO_2 mole fraction in liquid phase (x_{CO_2}) and glycerol mole fraction in the vapor phase ($y_{glycerol}$). *%AAD* for a variable z is defined as:

$$\%AADz = \frac{1}{N_p}\sum_{i=1}^{N_p}\left|\frac{z_i^{\exp} - z_i^{calc}}{z_i^{\exp}}\right| \times 100 \tag{17}$$

where N_p is the number of experimental values.

3. Results and discussion

3.1. Solubility of glycerol in the CO_2-rich phase

Fig. 1a shows the evolution of the infrared spectra in the spectral range 2800–3050 cm^{-1} of glycerol solubilized in the CO_2-rich phase with an increase of pressure from 10.0 to 35.0 MPa at 120 °C. a progressive increase of the peaks centered at 2883 cm^{-1} and 2933 cm^{-1} assigned to ν_{CH} of glycerol can be observed, resulting from the increase of glycerol concentration. From the intensity of both peaks, the evolution of the solubility of glycerol in the CO_2-rich phase as a function of CO_2 density at different temperatures (see Fig. 1b) has been calculated. As it can be observed, the values of solubility are very low, and increment of the CO_2 density increases the solubility of glycerol at a given temperature. In fact, glycerol is barely soluble in CO_2 at low temperatures and at constant density; a slight increment in temperature induces a significant increase of solubility. Our results are intermediate between the experimental results previously published by Sovova and Khachaturyan [17] and by Elssier and Friedrich [16], which presented a difference of two orders of magnitude between them. The authors have attributed this difference to a 0.37 wt% difference in the glycerol water content. However, it can be pointed out that the methods used in both studies can induce systematic errors, principally when solute solubility is small (as in the case of glycerol). In both publications, several points are not provided in details, such as analysis methods and equilibration time justification.

Table 5 shows the calculated mole fraction of glycerol in the CO_2-rich phase ($y_{glycerol}$) obtained from experimental results of the solubility presented in Fig. 1b.

As can be concluded from these values, a major advantage of the experimental method used in this study lies in its ability to measure very low values of concentration with an acceptable precision.

3.2. Solubility of CO_2 and swelling of glycerol in the glycerol-rich phase

As an example, Fig. 2 shows the spectral changes of the glycerol-rich phase occurring with an increase of temperature from 40 to 200 °C at 10.0 MPa as a result of the change in CO_2 concentration in that phase. The peak at 3696 cm^{-1}, assigned to the combination mode $2\nu_2 + \nu_3$ of the CO_2, decreases with temperature, which results from a decrease of CO_2 concentration in the glycerol-rich phase when temperature increases from 40 to 200 °C. The peak detected at 4740 cm^{-1}, assigned to the combination of the ν(OH) + δ(OH) mode of the associated OH of glycerol, presents a shift towards 4865 cm^{-1} (dashed lines) when temperature increases,

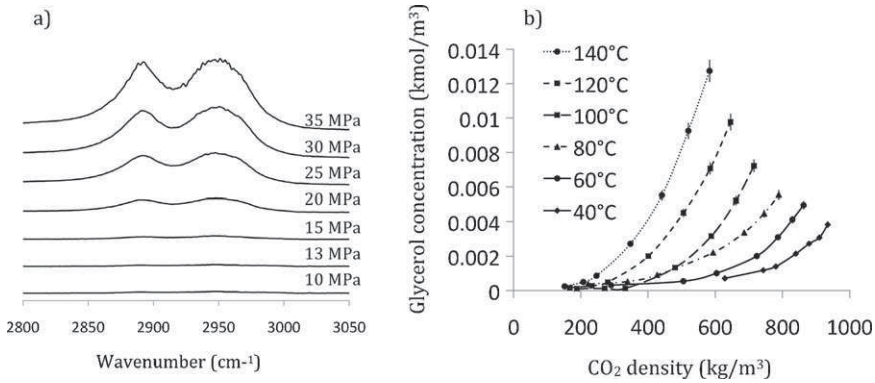

Figure 1. (a) Spectral changes of the CO_2-rich phase with the pressure at 120 °C. (b) Solubility of glycerol as a function of CO_2 molar density at temperatures between 40 °C and 140 °C. Lines have been added to guide the eye. Error bars represent the 5% of relative error allowed by our method.

Table 5
CO_2-rich phase equilibrium experimental data. S = solubility of glycerol in CO_2.

40 °C			60 °C			80 °C		
P (MPa)	$y_{glycerol}$	S (kmol/m^3)	P (MPa)	$y_{glycerol}$	S (kmol/m^3)	P (MPa)	$y_{glycerol}$	S (kmol/m^3)
10	4.95×10^{-5}	0.7×10^{-3}	10	4.70×10^{-5}	3.06×10^{-4}	10	7.41×10^{-5}	3.73×10^{-4}
13	6.96×10^{-5}	1.17×10^{-3}	13	4.70×10^{-5}	5.4×10^{-4}	13	6.80×10^{-5}	5.22×10^{-4}
15	7.84×10^{-5}	1.39×10^{-3}	15	7.29×10^{-5}	1.0×10^{-3}	15	9.33×10^{-5}	9.03×10^{-4}
20	1.12×10^{-4}	2.14×10^{-3}	20	1.22×10^{-4}	2.0×10^{-3}	20	1.63×10^{-4}	2.2×10^{-3}
25	1.36×10^{-4}	2.72×10^{-3}	25	1.73×10^{-4}	3.09×10^{-3}	25	2.16×10^{-4}	3.37×10^{-3}
30	1.49×10^{-4}	3.07×10^{-3}	30	2.19×10^{-4}	4.12×10^{-3}	30	2.64×10^{-4}	4.47×10^{-3}
35	1.80×10^{-4}	3.83×10^{-3}	35	2.53×10^{-4}	4.96×10^{-3}	35	3.09×10^{-4}	5.54×10^{-3}
100 °C			120 °C			140 °C		
P (MPa)	$y_{glycerol}$	S (kmol/m^3)	P (MPa)	$y_{glycerol}$	S (kmol/m^3)	P (MPa)	$y_{glycerol}$	S (kmol/m^3)
10	2.41×10^{-5}	1.06×10^{-4}	10	4.18×10^{-5}	1.59×10^{-4}	10	6.93×10^{-5}	2.39×10^{-4}
13	1.93×10^{-5}	1.2×10^{-4}	13	5.25×10^{-5}	2.78×10^{-4}	13	1.05×10^{-4}	4.97×10^{-4}
15	1.58×10^{-5}	1.22×10^{-4}	15	7.61×10^{-5}	4.85×10^{-4}	15	1.53×10^{-4}	8.59×10^{-4}
20	1.21×10^{-4}	1.33×10^{-3}	20	2.20×10^{-4}	2.0×10^{-3}	20	3.44×10^{-4}	2.71×10^{-3}
25	2.37×10^{-4}	3.17×10^{-3}	25	3.93×10^{-4}	4.51×10^{-3}	25	5.50×10^{-4}	5.52×10^{-3}
30	3.46×10^{-4}	5.21×10^{-3}	30	5.31×10^{-4}	7.07×10^{-3}	30	7.83×10^{-4}	9.26×10^{-3}
35	4.44×10^{-4}	7.22×10^{-3}	35	6.66×10^{-4}	9.77×10^{-3}	35	9.60×10^{-4}	1.27×10^{-2}

which results from a progressive breaking of the hydrogen bond network of glycerol molecules, as previously reported for other alcohols [22]. In fact, glycerol is a highly flexible molecule forming both intra- and inter-molecular hydrogen bonds; molecular dynamics simulations on this molecule have shown that the number of inter-molecular hydrogen bonds decreases when temperature is increased [43,44]. The intensity of the peak at 4350 cm^{-1} associated to a combination mode ν(CH) + δ(CH) decreases with temperature, as a result of the glycerol density decrease. No glycerol swelling, as a result of CO_2 solubilization, was observed during our experiments within the ±5% accuracy of our methodology as it is shown in Fig. 3. Indeed, no changes in the intensity of characteristic bands of glycerol are observed (bands around 4000 cm^{-1} and 4370 cm^{-1}) although an increase of the characteristic band of CO_2 (3696 cm^{-1}) with pressure is clearly present.

The solubility of CO_2 in the glycerol-rich phase is reported in kmol/m^3 in Fig. 4 as a function of the pressure. Table 6 presents the CO_2 mole fraction in the glycerol rich phase (x_{CO_2}) deduced

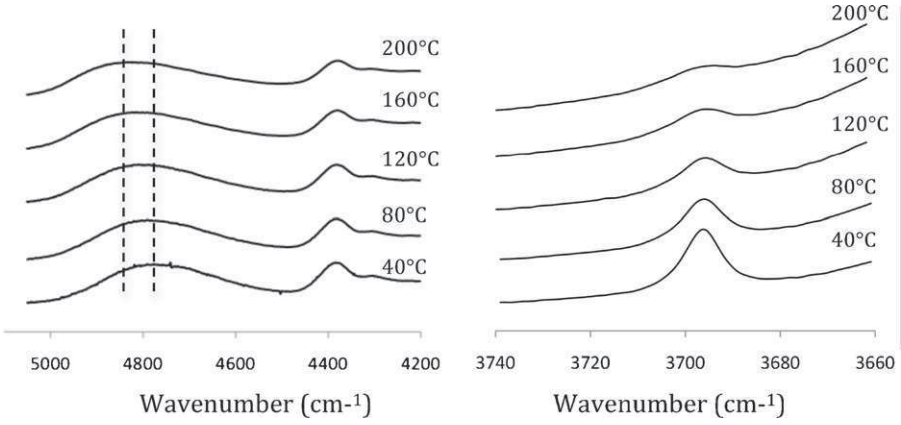

Figure 2. Spectral changes of the glycerol-rich phase with temperature at 10 MPa.

Table 6
Glycerol-rich phase equilibrium experimental data. S = solubility of CO_2 in glycerol.

40 °C			60 °C			80 °C		
P (MPa)	x_{CO_2}	S (kmol/m^3)	P (MPa)	x_{CO_2}	S (kmol/m^3)	P (MPa)	x_{CO_2}	S (kmol/m^3)
5	0.0834	1.25	5	0.0685	1.01	10	0.0807	1.2
7.8	0.1068	1.64	10	0.0981	1.49	15	0.0967	1.47
10	0.1170	1.82	15	0.1065	1.63	20	0.1015	1.55
15	0.1259	1.97	20	0.1114	1.72	30	0.1215	1.89
20	0.1280	2.01	24.9	0.1210	1.88			
30	0.1335	2.11	30	0.1215	1.89			
100 °C			120 °C			140 °C		
P (MPa)	x_{CO_2}	S (kmol/m^3)	P (MPa)	x_{CO_2}	S (kmol/m^3)	P (MPa)	x_{CO_2}	S (kmol/m^3)
10	0.0631	0.92	10.2	0.0538	0.78	10	0.0428	0.61
15	0.0753	1.11	15	0.0646	0.95	15	0.0539	0.78
20	0.0900	1.36	20	0.0816	1.22	20	0.0674	0.99
30	0.1183	1.84	24.8	0.0952	1.44	25	0.0922	1.39
			30	0.1132	1.75	30	0.1055	1.61
160 °C			180 °C			200 °C		
P (MPa)	x_{CO_2}	S (kmol/m^3)	P (MPa)	x_{CO_2}	S (kmol/m^3)	P (MPa)	x_{CO_2}	S (kmol/m^3)
10	0.0334	0.47	10	0.0246	0.35	10.2	0.0203	0.28
15	0.0442	0.63	15	0.0369	0.52	15	0.0242	0.34
20	0.0577	0.84	20	0.0470	0.68	20.2	0.0383	0.55
25	0.0821	1.23	25	0.0677	0.99	30	0.087	
30	0.0966	1.46	30	0.0875	1.31			

from experimental data of solubility. In all cases, at a given temperature, solubility increases with pressure. Nevertheless, at low temperature (T = 40 °C), there is a strong increase of the solubility when pressure is increased, up to 10 MPa. For greater pressures, this effect is leveled off. As temperatures increases, a more important effect of pressure has been observed, and at T = 200 °C, this effect is maximal. In all cases, temperature has a negative effect on solubility of CO_2 in glycerol in the temperature and pressure ranges studied. It can be observed that the shape of the curves of CO_2 solubility as a function of the pressure is different above 140 °C. This behavior may be the consequence of a significant weakening of the hydrogen bonded structure of glycerol above this temperature.

3.3. Phase diagram of the $scCO_2$/glycerol system

3.3.1. Experimental results

Phase diagram for the CO_2–glycerol system has been obtained from solubility measurements for temperatures ranging from 40 °C to 200 °C and pressures up to 35 MPa and is presented in Fig. 5a. As described above, quite low mutual solubility is observed between CO_2 and glycerol in the pressure and temperature ranges studied here. In the case of the glycerol-rich phase, low quantities of CO_2 can be dissolved. However, at 30 MPa and 40 °C, a CO_2 mole fraction of up to 0.13 (Fig. 5b) can be obtained.

Concerning the CO_2-rich phase, whatever the temperature, the quasi-vertical line reveals the low solubility of glycerol in CO_2; a closer look on Fig. 5c indicates an important effect of temperature on glycerol solubility. This behavior is typical for binary systems with compounds of widely different molar mass and/or critical temperatures, such as CO_2/water or CO_2/glycol systems. Such systems exhibit a liquid–liquid immiscibility zone at low temperatures and belong to type III of the classification of Scott and Konynenburg [45,46]. The low solubility of glycerol in the CO_2 rich phase is an important characteristic in respect to the development of biphasic reactive systems using glycerol as the catalytic phase and $scCO_2$ as the reactants and products carrier [12]. Indeed, this insures that low amounts of glycerol are extracted by $scCO_2$ during the separation step.

3.3.2. Phase equilibrium modeling

Models of Table 4 have been used to describe fluid phase equilibrium of the CO_2/glycerol system. As previously mentioned,

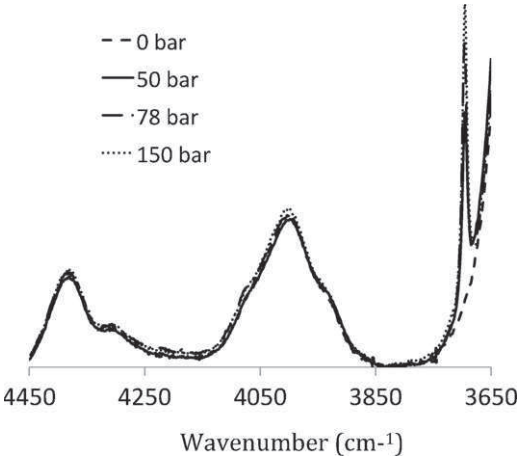

Figure 3. Spectral changes of the glycerol-rich phase with pressure at 40 °C.

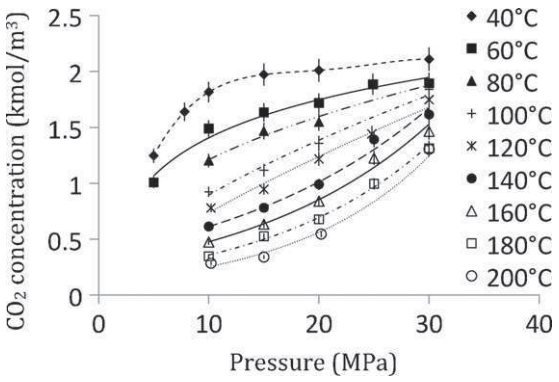

Figure 4. Solubility of CO_2 in glycerol as a function of pressure at T = 40–200 °C. Lines have been added to guide the eye. Error bars represent the 5% of relative error allowed by our method.

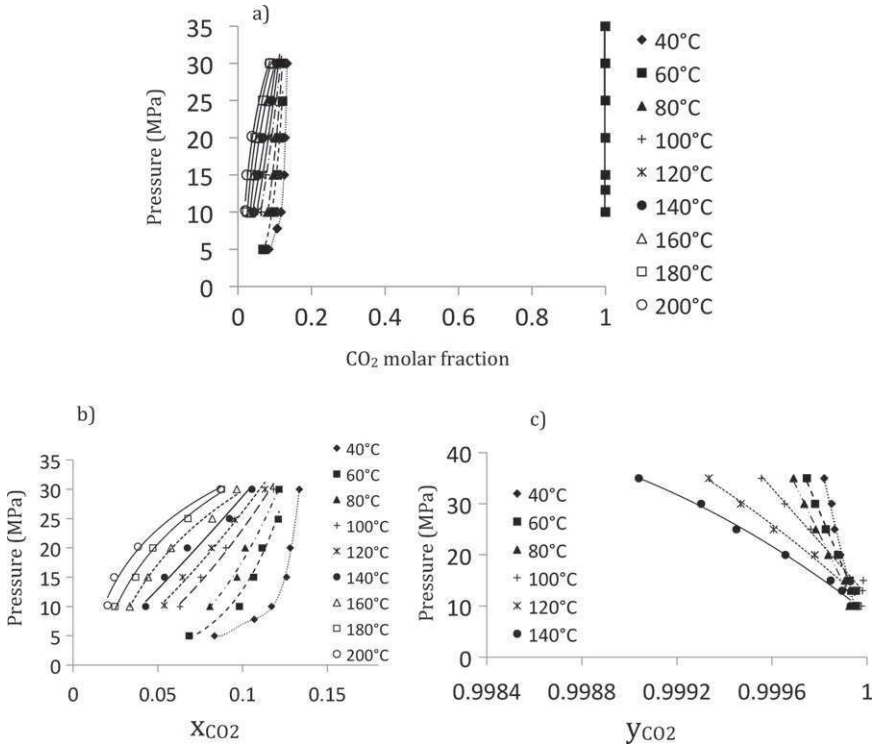

Figure 5. (a) Pressure *versus* CO_2 mole fraction diagram for the $scCO_2$/glycerol system. (b) Glycerol-rich phase and (c) CO_2-rich phase. Lines have been added to guide the eye.

PSRK-UNIFAC and MHV2-UNIFAC models are predictive, while for PSRK-UNIQUAC and MHV2-UNIQUAC models binary interaction parameters have to be fitted from experimental data. Values of global absolute average deviations, $\%AAD_{xCO_2}$ and $\%AAD_{y_{glycerol}}$ (Eq. (17)), obtained for each model, together with expressions of fitted binary interaction parameters are given in Table 7. The fitting of experimental data has been done minimizing an objective function (least square method) and results are presented in Table 7 where it is first noticeable that, whatever the model used, the *%AAD* on both phases are not very good, none of them being below 5%. This shows that, on a global point of view, PR EoS fails to accurately represent experimental behavior of that system, even with EoS/G^E mixing rules.

For the PR EoS with classical mixing rule, it has not been possible to use an objective function simultaneously involving composition of liquid phase and composition of the vapor phase in the same resolution, because in that case, it led to globally poor description for both phases. Especially, the very low experimental mole fractions of glycerol in the CO_2 rich phase were systematically largely overestimated. Thus for PR model with classical mixing rule, the optimization method was done firstly with the least square method applied to x_{CO_2} values only (entry 1), that explains the rather satisfactory value of *%AAD* (7.7) for the glycerol rich phase in that case; Then the fitting was done on $y_{glycerol}$ only (entry 2), giving acceptable *%AAD* for the vapor phase (61.1, still overestimating the

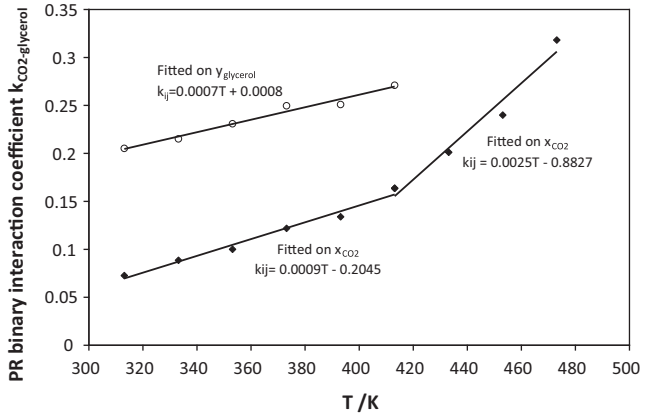

Figure 6. Influence of the temperature on binary interaction coefficients of Peng–Robinson equation of state fitted on x_{CO_2} or $y_{glycerol}$.

Table 7
Values of binary interaction coefficients and corresponding values of the relative absolute average deviations (*%AAD*) for CO_2 liquid mole fraction and glycerol vapor mole fraction for each model.

Entry	Global model	Binary interaction parameters	$\%AAD_{xCO_2}$	$\%AAD_{y_{glycerol}}$
1	PR fitted on x_{CO_2} only	$k_{CO_2-glycerol} = 0.009T/K - 0.2075$ for $T \leq 413\,K$ $k_{CO_2-glycerol} = 0.025T/K - 0.8827$ for $T > 413\,K$	7.7	345
2	PR fitted on $y_{glycerol}$ only	$k_{CO_2-glycerol} = 0.0007T/K + 0.0008$	62.2	61.1
3	PSRK-UNIQUAC fitted on both x_{CO_2} and $y_{glycerol}$	$A_{CO_2-glycerol}/cal\ mol^{-1} = -3.00T/K + 1523.31$ $A_{glycerol-CO_2}/cal\ mol^{-1} = 3.84T/K - 1056.75$	18.4	57.2
4	PSRK-UNIFAC	–	71.3	297.1
5	MHV2-UNIQUAC fitted on both x_{CO_2} and $y_{glycerol}$	$A_{CO_2-glycerol}/cal\ mol^{-1} = 75,698.7T/K + 358.30$ $A_{glycerol-CO_2}/cal\ mol^{-1} = -2.81T/K + 2109.18$	19.5	97.5
6	MHV2-UNIFAC	–	280.3	815.7

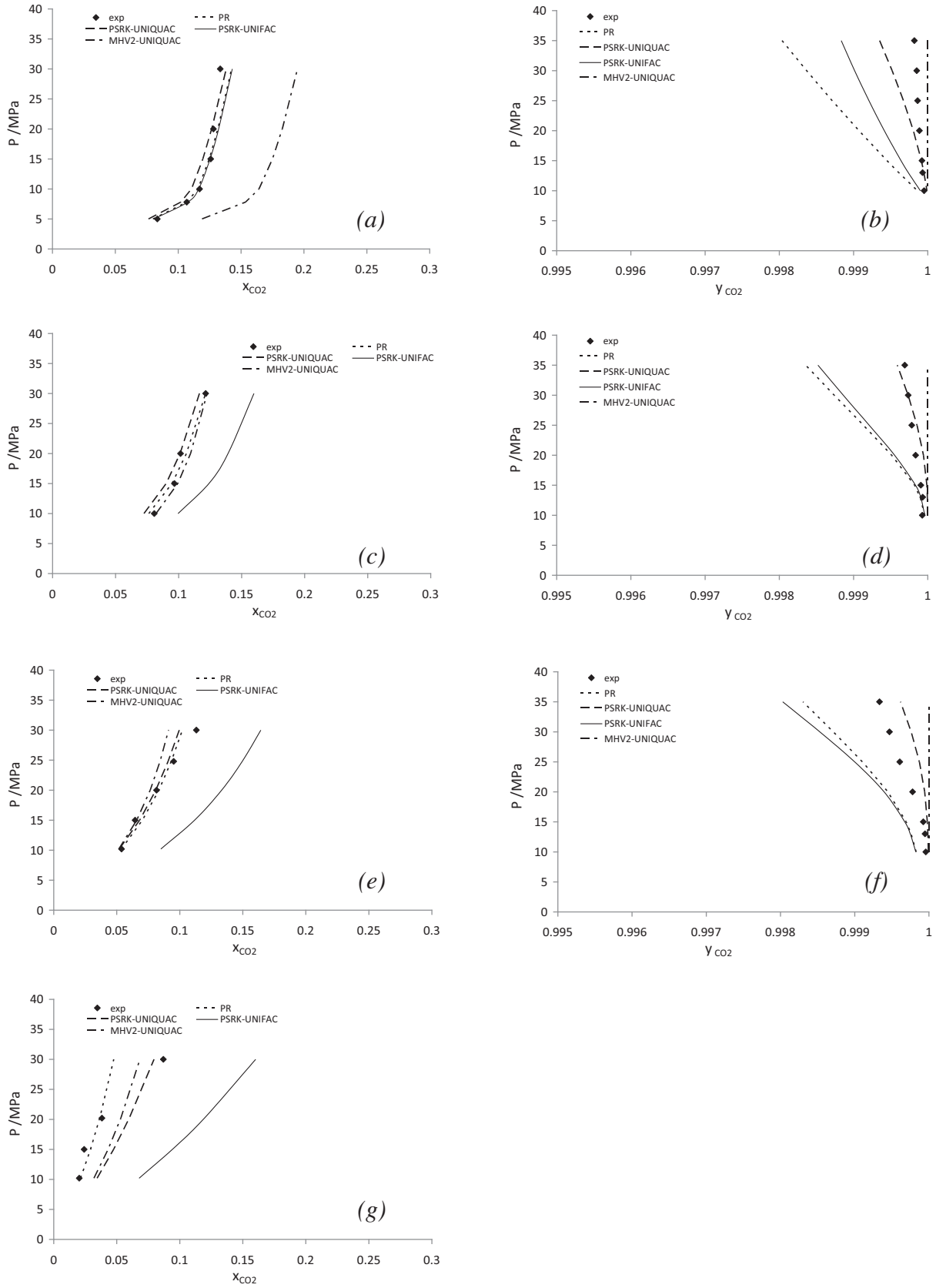

Figure 7. P-*x*,*y* data for the CO_2/glycerol system, experimental data and modeling results. (a and b) 40 °C, (c and d) 80 °C, (e and f) 120 °C, (g) 200 °C (k_{ij} for PR EoS is from Table 7, entry 1).

glycerol mole fraction), but, in this case worse predictions were correlatively found for the liquid phase (62.2). In the case of PR EoS, a detailed study of the influence of temperature upon binary interaction coefficients has been done and results are plotted in Fig. 6. When fitting was realized on x_{CO_2} only, two linear correlations have been evidenced, depending on the temperature range. Whatever the temperature, the k_{ij} value of the PR EoS is positive for this system, as it is often the case because of overestimation of interaction between molecules issued from the use of geometric mixing rule (Eq. (3)). Moreover, the value of k_{ij} increases with temperature, reflecting the decrease of the solubility of CO_2 into the glycerol rich phase and the increase of solubility of glycerol into CO_2 rich phase, because self-association of glycerol by hydrogen bonding is weaker at high temperature, as previously mentioned. As can be seen in Fig. 6, influence of temperature on k_{ij} is more important above 140 °C and this is presumably a consequence of the observed change of the mixture behavior above 140 °C, as it is clearly observable in Fig. 4, where a change of concavity occurs when solubility of CO_2 in glycerol rich phase *versus* pressure is plotted. The similar analysis on k_{ij} fitted on $y_{glycerol}$ shows that, at a same temperature, k_{ij} value is higher, and the same tendency is observed as a function of the temperature (Fig. 6). Note that experimental vapor phase compositions have been determined for $T < 140$ °C only. For the purpose of the targeted application of the CO_2–glycerol system as a biphasic medium to perform reactions, information upon the amount of CO_2 solubilized in glycerol is of prime interest because of the consequences upon physico-chemical properties or reactivity in the glycerol rich phase. Inaccurate prediction of the traces of glycerol in the CO_2 rich phase would not handicap the development of such biphasic systems. Thus, in the following, the results with PR EoS and k_{ij} fitted on x_{CO_2} only have been retained. The approach which privileges the vapor phase description could be proposed in the context of an application where an accurate calculation of the vapor phase composition is needed. However, as can be seen in Table 7, when a description for both phases simultaneously is needed the PSRK-UNIQUAC should be preferred (entry 3) because it gives acceptable *%AAD* (18.4 and 57.2 for x_{CO_2} and $y_{glycerol}$ respectively) although there is a loss of accuracy for the liquid phase in comparison to entry 1. Visual assessment of calculated and experimental CO_2 mole fractions in the glycerol rich phase can be done in Fig. 7(a), (c), (e) and (g), and in the CO_2 rich phase in Fig. 7(b), (d) and (f), at 40, 80, 120 and 200 °C. Among mixing rules based on EoS/G^E approach, it appears clearly that PSRK mixing rule with UNIQUAC activity model provides the best results in terms of both liquid and vapor compositions, followed by MHV2 mixing rule with UNIQUAC (entry 5), that gives worse results. Although the deviations obtained with PSRK-UNIQUAC are still rather high, this result confirms that these mixing rules are the most adequate to predict experimental behavior of such complex mixtures, as compared to classical vdW1f mixing rules. Essentially, the high values of deviations may be explained by the large difference of CO_2 and glycerol critical volumes (94 $cm^3\,mol^{-1}$ and 264 $cm^3\,mol^{-1}$, respectively). Indeed, the CO_2–glycerol mixture could be classified as a size-asymmetric system, for which it has been shown that this kind of model is actually somewhat unsuitable [47], due to the difference between the combinatorial term of the activity coefficient model and the one of the equation of state. This difference increases as the difference in molecule size increases [47].

To better investigate the ability of the models to represent global experimental behavior of the liquid phase of the CO_2/glycerol system on the wide range of temperature, it is interesting to consider variations of *%AADx* obtained with the different models with the temperature (Fig. 8) (*Note*: MHV2-UNIFAC is not considered because *%AADx* is very high, whatever the temperature).

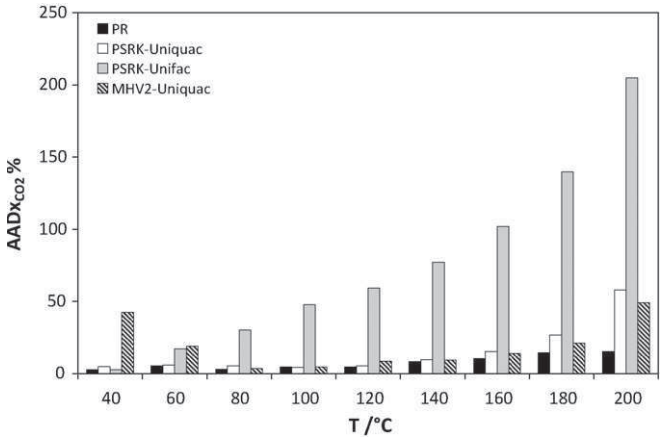

Figure 8. Influence of the temperature on *%AAD* for x_{CO_2} obtained with different models.

Several tendencies can be observed from Figs. 7 and 8. Firstly, as previously pointed out, whatever the temperature, non-predictive models with fitted binary interaction parameters are the most suitable. Of course, this result was expected, considering the fact that for these models four coefficients are fitted to experimental data in order to minimize global average deviation. It is shown in Fig. 8 that deviations are higher at high temperature, where the experimental curves show a change in concavity and where experimental points are scarce.

Essentially, predictive models, *i.e.*, models using UNIFAC in mixing rules, yielded poor representation of experimental results, particularly MHV2-UNIFAC (Table 7, entry 6). PSRK-UNIFAC approach is satisfactory at low temperature, but deviation sharply increases with temperature to reach about 200% at 200 °C (Fig. 8). Concerning this last model, this result was expected considering the fact that, for the functional groups of our database used to describe the CO_2/glycerol system (*i.e.*, CO_2, OH and CH_2 functional groups), binary interaction parameters within these groups are provided as temperature independent.

PSRK mixing rule was found here superior to MHV2, whatever the activity coefficient model, UNIFAC or UNIQUAC, chosen in the mixing rule. This result is somewhat surprising, because MHV2 mixing rule provides generally a better match of experimental results.

The thermodynamic behavior of CO_2/glycerol system is obviously governed by self-interaction of glycerol. For such a system, an improvement in phase equilibrium modeling could be achieved by using advanced models based on association theories, such as SAFT (Statistical Associating Fluid Theory) or CPA (Cubic Plus Association) models. Although grounded on a more complex theoretical basis, these models have been proved to be particularly suitable for associating compounds [34].

4. Conclusions

In this work, the mutual solubility of CO_2 and glycerol has been studied at temperatures ranging from 40 °C to 200 °C and pressures up to 35.0 MPa. This has been done using the FT-IR technique which proved to give access to very low values of equilibrium concentrations with a good accuracy. Concerning the CO_2 rich phase, it was observed that the glycerol solubility in CO_2 was extremely low (in the range of 10^{-5} in mole fraction) in the pressure and temperature domains investigated here. Conversely, the glycerol rich phase dissolved CO_2 at mole fractions up to 0.13. Negligible swelling of the glycerol rich phase has been observed, which indicates that glycerol behaves as a class I Gas Expanded Liquid (GXL)

according to the classification of Jessop et al. [1], *i.e.*, a system where the expanding gas has a quite low solubility in the liquid, which consequently does not exhibit large expansion. Although the solubility of CO_2 in glycerol is largely higher than the one of CO_2 in water, the thermodynamic behavior of this system is rather similar to that of CO_2/water binary mixture, which is a class I GXL.

Concerning the modeling of the CO_2/glycerol system, the suitability of PR EoS with PSRK mixing rule and UNIQUAC model, has been highlighted. Evolution with pressure of the composition of both phases in the 40–200 °C range of temperature is quite well described by this model, provided that suitable values of binary interaction coefficients are used. Conversely, predictive approaches proved to be non satisfactory. Simpler approach with Peng–Robinson equation of state with vdW1f mixing rule did not allow computing accurately both liquid and vapor phases with the same value of binary interaction coefficient. Depending on the application, accurate description of only one specific phase could be needed. In this work, an adapted fitting procedure that has considered only the targeted phase, have provided the specific interaction coefficients for each case.

This study has also shown that the system $scCO_2$/glycerol remained biphasic for all studied pressures and temperatures, allowing further development of biphasic reaction systems, which involve environmentally friendly solvents only. These systems also make it possible to couple reaction and separation steps, allowing the development of intensified processes.

References

[1] P.G. Jessop, B. Subramaniam, Gas-expanded liquids, Chemical Reviews 107 (2007) 2666–2694.
[2] G.R. Akien, M. Poliakoff, A critical look at reactions in class I and II gas-expanded liquids using CO_2 and other gases, Green Chemistry 11 (2009) 1083–1100.
[3] A. Wolfson, C. Dlugy, Palladium-catalyzed Heck and Suzuki coupling in glycerol, Chemical Papers 61 (2007) 228–232.
[4] A. Wolfson, C. Dlugy, Y. Shotland, Glycerol as a green solvent for high product yields and selectivities, Environmental Chemistry Letters 5 (2007) 67–71.
[5] A. Wolfson, C. Dlugy, Glycerol as an alternative green medium for carbonyl compound reductions, Organic Communications 2 (2009) 34.
[6] A.E. Diaz-Alvarez, J. Francos, B. Lastra-Barreira, P. Crochet, V. Cadierno, Glycerol and derived solvents: new sustainable reaction media for organic synthesis, Chemical Communications 47 (2011) 6208–6227.
[7] Y. Gu, J. Barrault, F. Jérôme, Glycerol as an efficient promoting medium for organic reactions, Advanced Synthesis & Catalysis 350 (2008) 2007–2012.
[8] F. Jérôme, Y. Pouilloux, J. Barrault, Rational design of solid catalysts for the selective use of glycerol as a natural organic building block, ChemSusChem 1 (2008) 586–613.
[9] Y. Gu, F. Jerome, Glycerol as a sustainable solvent for green chemistry, Green Chemistry 12 (2010) 1127–1138.
[10] A. Karam, N. Villandier, M. Delample, C.K. Koerkamp, J.-P. Douliez, R. Granet, P. Krausz, J. Barrault, F. Jérôme, Rational design of sugar-based-surfactant combined catalysts for promoting glycerol as a solvent, Chemistry: A European J. 14 (2008) 10196–10200.
[11] R.A. Sheldon, Green solvents for sustainable organic synthesis: state of the art, Green Chemistry 7 (2005) 267–278.
[12] M. Delample, N. Villandier, J.-P. Douliez, S. Camy, J.-S. Condoret, Y. Pouilloux, J. Barrault, F. Jerome, Glycerol as a cheap, safe and sustainable solvent for the catalytic and regioselective β,β-diarylation of acrylates over palladium nanoparticles, Green Chemistry 12 (2010) 804–808.
[13] P. Licence, M.P. Dellar, R.G.M. Wilson, P.A. Fields, D. Litchfield, H.M. Woods, M. Poliakoff, S.M. Howdle, Large-aperture variable-volume view cell for the determination of phase-equilibria in high pressure systems and supercritical fluids, Review of Scientific Instruments 75 (2004) 3233–3236.
[14] A.A. Novitskiy, E. Pérez, W. Wu, J. Ke, M. Poliakoff, A new continuous method for performing rapid phase equilibrium measurements on binary mixtures containing CO_2 or H_2O at high pressures and temperatures, J. Chemical & Engineering Data 54 (2009) 1580–1584.
[15] A.P. Abbott, E.G. Hope, R. Mistry, A.M. Stuart, Controlling phase behaviour on gas expansion of fluid mixtures, Green Chemistry 11 (2009) 1536–1540.
[16] R. Elssier, J. Friedrich, Estimation of supercritical fluid-liquid solubility parameter differences for vegetable oils and other liquids from data taken with a stirred autoclave, J. American Oil Chemists' Society 65 (1988) 764–767.
[17] H. Sovova, J. Jez, M. Khachaturyan, Solubility of squalane, dinonyl phthalate and glycerol in supercritical CO_2, Fluid Phase Equilibria 137 (1997) 185–191.
[18] S. Foltran, L. Maisonneuve, E. Cloutet, B. Gadenne, C. Alfos, T. Tassaing, H. Cramail, Solubility in CO_2 and swelling studies by in situ IR spectroscopy of vegetable-based epoxidized oils as polyurethane precursors, Polymer Chemistry 3 (2012) 525–532.
[19] S. Foltran, E. Cloutet, H. Cramail, T. Tassaing, In situ FTIR investigation of the solubility and swelling of model epoxides in supercritical CO_2, J. Supercritical Fluids 63 (2012) 52–58.
[20] T. Guadagno, S.G. Kazarian, High-pressure CO_2-expanded solvents: simultaneous measurement of CO_2 sorption and swelling of liquid polymers with in-situ near-IR spectroscopy, J. Physical Chemistry B 108 (2004) 13995–13999.
[21] P. Vitoux, T. Tassaing, F. Cansell, S. Marre, C. Aymonier, In situ IR spectroscopy and ab initio calculations to study polymer swelling by supercritical CO_2, J. Physical Chemistry B 113 (2009) 897–905.
[22] F. Palombo, T. Tassaing, Y. Danten, M. Besnard, Hydrogen bonding in liquid and supercritical 1-octanol and 2-octanol assessed by near and midinfrared spectroscopy, J. Chemical Physics 125 (2006) 094503.
[23] R. Oparin, T. Tassaing, Y. Danten, M. Besnard, Structural evolution of aqueous NaCl solutions dissolved in supercritical carbon dioxide under isobaric heating by mid and near infrared spectroscopy, J. Chemical Physics 122 (2005) 094505.
[24] M. Buback, J. Schweer, H. Yups, New infrared absorption of pure carbon dioxide up to 3100 bar and 500 K. Wavenumber range 3200 cm^{-1} to 5600^{-1}, Zeitschrift für Naturforschung A 41a (1986) 505–511.
[25] J.M. Lopes, Z. Petrovski, R. Bogel-Lukasik, E. Bogel-Lukasik, Heterogeneous palladium-catalyzed telomerization of myrcene with glycerol derivatives in supercritical carbon dioxide: a facile route to new building blocks, Green Chemistry 13 (2011) 2013–2016.
[26] National Institute of Standards and Technology, http://webbook.nist.gov/chemistry/
[27] H. Khelladi, F.d.r. Plantier, J.L. Daridon, H. Djelouah, Measurement under high pressure of the nonlinearity parameter B/A in glycerol at various temperatures, Ultrasonics 49 (2009) 668–675.
[28] D.-Y. Peng, D.B. Robinson, A new two-constant equation of state, Industrial & Engineering Chemistry Fundamentals 15 (1976) 59–64.
[29] D.-Y. Peng, D.B. Robinon, The Characterization of the Heptanes and Heavier Fractions for the GPA Peng–Robinson Programs, Gas Processors Association, Research Report PR-28, 1978.
[30] J.F. Boston, P.M. Mathias, Phase equilibria in a third-generation process simulator, in: Proceedings of the 2nd International Conference on Phase Equilibria and Fluid Properties in the Chemical Process Industries, West Berlin, 17–21 March, 1980, pp. 823–849.
[31] M.-J. Huron, J. Vidal, New mixing rules in simple equations of state for representing vapour–liquid equilibria of strongly non-ideal mixtures, Fluid Phase Equilibria 3 (1979) 255–271.
[32] K. Knudsen, L. Coniglio, R. Gani, Correlation and prediction of phase equilibria of mixtures with supercritical compounds for a class of equations of state, in: Innovations in Supercritical Fluids, American Chemical Society, Washington, DC, 1995, pp. 140–153.
[33] S. Camy, J.S. Pic, E. Badens, J.S. Condoret, Fluid phase equilibria of the reacting mixture in the dimethyl carbonate synthesis from supercritical CO_2, J. Supercritical Fluids 25 (2003) 19–32.
[34] G.M. Kontogeorgis, G.K. Folas, Thermodynamic Models for Industrial Applications: From Classical and Advanced Mixing Rules to Association Theories, John Wiley & Sons Ltd., Chichester, 2010.
[35] T. Holderbaum, J. Gmehling, PSRK: a group contribution equation of state based on UNIFAC, Fluid Phase Equilibria 70 (1991) 251–265.
[36] M.L. Michelsen, A method for incorporating excess Gibbs energy models in equations of state, Fluid Phase Equilibria 60 (1990) 47–58.
[37] S. Dahl, M.L. Michelsen, High-pressure vapor–liquid equilibrium with a UNIFAC-based equation of state, American Institute of Chemical Engineers J. 36 (1990) 1829–1836.
[38] A. Fredenslund, R.L. Jones, J.M. Prausnitz, Group-contribution estimation of activity coefficients in nonideal liquid mixtures, American Institute of Chemical Engineers J. 21 (1975) 1086–1099.
[39] K. Fischer, J. Gmehling, Further development, status and results of the PSRK method for the prediction of vapor–liquid equilibria and gas solubilities, Fluid Phase Equilibria 121 (1996) 185–206.
[40] D.S. Abrams, J.M. Prausnitz, Statistical thermodynamics of liquid mixtures: a new expression for the excess Gibbs energy of partly or completely miscible systems, American Institute of Chemical Engineers J. 21 (1975) 116–128.
[41] T.F. Anderson, J.M. Prausnitz, Application of the UNIQUAC equation to calculation of multicomponent phase equilibria. 1. Vapor–liquid equilibria, Industrial & Engineering Chemistry Process Design and Development 17 (1978) 552–561.
[42] B.L. Larsen, P. Rasmussen, A. Fredenslund, A modified UNIFAC group-contribution model for prediction of phase equilibria and heats of mixing, Industrial & Engineering Chemistry Research 26 (1987) 2274–2286.
[43] R. Chelli, P. Procacci, G. Cardini, S. Califano, Glycerol condensed phases. Part II. A molecular dynamics study of the conformational structure and hydrogen bonding, Physical Chemistry Chemical Physics 1 (1999) 879–885.
[44] R. Chelli, F.L. Gervasio, C. Gellini, P. Procacci, G. Cardini, V. Schettino, Density functional calculation of structural and vibrational properties of glycerol, J. Physical Chemistry A 104 (2000) 5351–5357.
[45] M.B. King, A. Mubarak, J.D. Kim, T.R. Bott, The mutual solubilities of water with supercritical and liquid carbon dioxides, J. Supercritical Fluids 5 (1992) 296–302.
[46] P.H.V. Konynenburg, R.L. Scott, Critical lines and phase equilibria in binary Van Der Waals mixtures, Philosophical Transactions of the Royal Society of London. Series A: Mathematical and Physical Sciences 298 (1980) 495–540.

[47] G.M. Kontogeorgis, P.M. Vlamos, An interpretation of the behavior of EoS/G^E models for asymmetric systems, Chemical Engineering Science 55 (2000) 2351–2358.
[48] C.S. Miner, N.N. Dalton (Eds.), Glycerol, American Chemical Society Monograph Series, vol. 42, Reinhold Publishing Corp., New York, 1953, p. 326.
[49] O.A.S. Araujo, P.M. Ndiaye, L.P. Ramos, M.L. Corazza, Phase behavior measurement for the system CO_2 + glycerol + ethanol at high pressures, J. Supercritical Fluids 62 (2012) 41–46.
[50] Y. Shimoyama, T. Abeta, L. Zhao, Y. Iwai, Measurement and calculation of vapor–liquid equilibria for methanol + glycerol and ethanol + glycerol systems at 493–573 K, Fluid Phase Equilibria 284 (2009) 64–69.